PROTEINS
STRUCTURE ■ FUNCTION ■ BIOINFORMATICS

Examination of the dynamic assembly equilibrium for *E. coli* ClpB

JiaBei Lin and Aaron L. Lucius*

Department of Chemistry, University of Alabama at Birmingham, Birmingham, Alabama 35294

ABSTRACT

***Escherichia coli* ClpB is a heat shock protein that belongs to the AAA+ protein superfamily. Studies have shown that ClpB and its homologue in yeast, Hsp104, can disrupt protein aggregates *in vivo*. It is thought that ClpB requires binding of nucleoside triphosphate to assemble into hexameric rings with protein binding activity. In addition, it is widely assumed that ClpB is uniformly hexameric in the presence of nucleotides. Here we report, in the absence of nucleotide, that increasing ClpB concentration leads to ClpB hexamer formation, decreasing NaCl concentration stabilizes ClpB hexamers, and the ClpB assembly reaction is best described by a monomer, dimer, tetramer, hexamer equilibrium under the three salt concentrations examined. Further, we found that ClpB oligomers exhibit relatively fast dissociation on the time scale of sedimentation. We anticipate our studies on ClpB assembly to be a starting point to understand how ClpB assembly is linked to the binding and disaggregation of denatured proteins.**

Proteins 2015; 83:2008–2024.

Key words: chaperones; thermodynamics; kinetics; AAA+ motor proteins; hexamer; analytical ultracentrifugation; Sedfit; SedAnal; protein unfoldases; protein quality control.

INTRODUCTION

The *Escherichia coli* ClpB (Caseinolytic peptidase B) protein belongs to the AAA+ (ATPase Associated with various cellular Activities) superfamily of ATPases.[1,2] Proteins in this family bind and hydrolyze ATP and utilize the energy to perform their cellular activities. These activities include folding and unfolding of proteins, dissociating protein–protein complexes, unwinding double stranded DNA, cytoskeleton regulation, and associating with proteases to form ATP-dependent proteases.[3]

As protein chaperones, ClpB and its eukaryotic ortholog, Hsp104, facilitate the dissociation of large protein aggregates in collaboration with the DnaK/Hsp70 system.[4–6] The disaggregation activity of ClpB and Hsp104 is essential for cell survival under stress. Their homologues have been found in plants and mitochondria, but not in the mammalian cytosol.[7] To date, the mechanism of ClpB catalyzed protein disaggregation is not fully understood. Understanding the ClpB disaggregation mechanism may aid in developing treatments for a variety of human neurodegenerative diseases that involve protein aggregation.[8,9]

In many cases, proteins in the AAA+ family assemble into hexamers or higher order oligomers when they bind nucleoside triphosphate. Although it is well established that ClpB, with two nucleotide binding domains (NBDs) per monomer, forms hexamers in the presence of nucleoside triphosphate,[10] an accurate model for ClpB assembly in the absence of nucleotide is lacking. This information will be required to quantitatively analyze the binding of nucleotide to the 12 ATP binding sites in the hexamer, address such questions as cooperativity between sites, and examine the subsequent linkage to polypeptide binding. This is because modeling the ligand-linked assembly process first requires an accurate model for the association equilibrium in the absence of the ligand.[11,12] Consequently, there is a need to determine what oligomers reside in solution and the self-association equilibrium constants that govern the population. Importantly, with the assembly energetics in hand, a precise determination of the concentration of hexamers as a function of both

Additional Supporting Information may be found in the online version of this article.

Grant sponsor: NSF; Grant number: MCB-1412624.

*Correspondence to: Aaron L. Lucius, Department of Chemistry, University of Alabama at Birmingham, 1530 3rd Avenue S, Birmingham, AL 35294.
E-mail:allucius@uab.edu

Received 23 June 2015; Revised 3 August 2015; Accepted 18 August 2015
Published online 27 August 2015 in Wiley Online Library (wileyonlinelibrary.com). DOI: 10.1002/prot.24914

nucleotide and ClpB concentration will be possible, which is essential for the quantitative interpretation of a vast array of *in vitro* studies.

Multiple reports show that ClpB resides in a dynamic equilibrium of monomers and hexamers or other oligomeric states.[10,13,14] Likely, due to the complexity of the assembly, conflicting reports have been presented as to whether or not ClpB forms hexamers or heptamers in the absence of nucleotide.[13–16] Zolkiewski *et al.* concluded that ClpB resides in a monomer-dimer-heptamer equilibrium.[10] Whereas, del Castillo *et al.* reported that ClpB assembly can best be described by a monomer-hexamer-dodecamer model.[10,13,14]

On the other hand, in the presence of nucleoside triphosphate, Zolkiewski *et al.* concluded that only hexamers were observed in their sedimentation equilibrium study which was performed with a single ClpB concentration.[10] Using gel filtration chromatography, Zolkiewski *et al.*,[10] Schlee *et al.*,[17] and Mogk *et al.*[18] reported chromatograms with broad elution peaks for ClpB in the presence of a large excess of ATP, indicating that either hexamers are dissociating during the gel filtration run, other oligomers are present in solution, or interactions with the media are occuring.[10]

In support of the interpretation that ClpB resides in a dynamic equilibrium, Werbeck *et al.* showed that ClpB exhibited what they describe as fast subunit exchange.[19] They used stopped-flow FRET experiments to show that *T. thermophilus* ClpB hexamers (or other oligomers) exhibit rapid subunit exchange both in the presence and absence of nucleotide. Despite the clear evidence that ClpB does not form stable hexamers, it is widely reported that only hexamers reside in solution in experiments performed at a variety of ClpB concentrations.[19–22]

Rapid subunit exchange is being reported to be an important aspect of the ClpB catalyzed protein disaggregation mechanism.[9,19,22] The hypothesis is that the hexameric ring that encounters a stable aggregate will tend to disassemble instead of stalling. In addition, hexamer is reported as the active conformation for its chaperon activity; therefore, it is imperative to fully understand both the association equilibria and kinetics for ClpB in the presence and absence of nucleoside triphosphate.

Here we report a quantitative examination of the self-association equilibrium for *E. coli* ClpB in the absence of nucleotide. Our results show that ClpB resides in a monomer-dimer-tetramer-hexamer equilibrium with no evidence found for the previously reported heptamers. We report the self-association equilibrium constants for each of these oligomers. Furthermore, the dissociation kinetics for ClpB are incorporated into the data analysis. The dissociation rate constant for each oligomer was found to be around or $>0.01\ s^{-1}$ in buffer H supplemented with 200 or 300 m*M* NaCl, indicating that *E. coli* ClpB oligomers dissociate on the time scale of minutes or shorter. In buffer H with 100 m*M* NaCl, the dissociation rate constant for ClpB hexamer was measured to be 1.3 (1.0, 1.6) $\times\ 10^{-3}\ s^{-1}$, indicating dissociation is slower but still on the time scale of minutes. Going forward, these results will make it possible to quantitatively examine the linkage of nucleotide binding to hexamer formation. This will make it possible to predict the concentration of hexamers as a function of both nucleotide and ClpB concentrations. Moreover, it will allow us to test the hypothesis that disassembly is a component of the ClpB catalyzed protein disaggregation reaction.

MATERIALS AND METHODS

Buffers

Buffers were prepared with reagent grade chemicals using deionized H_2O purified using the Purelab Ultra Genetic system (Siemens Water Technology). Buffer B is composed of 40 m*M* Tris, 2 m*M* 2-mercaptoethanol, and 10% (v/v) glycerol, pH 7.5 at 4°C. Buffer H contains 25 m*M* HEPES pH 7.5 at 25°C, 10 m*M* $MgCl_2$, 2 m*M* 2-mercaptoethanol, 10% (v/v) glycerol. The NaCl concentration is indicated in the text. All experiments were performed in buffer H, which contains 10% glycerol. The 10% glycerol is maintained in this work so that identical solution conditions are used as those used to examine polypeptide binding and translocation in our recent reports.[23,24] All ClpB concentrations referred to in the text are in monomeric units unless otherwise stated.

Strains, plasmid, and ClpB protein

The *E. coli* strains used were BL21 (DE3) and DH5α^{TM} (Invitrogen). The gene encoding for the N-terminally His_6-tagged *E. coli* ClpB (95 kDa) with thrombin cleavage site was cloned into the pET28b (+) vector (Novagen) and verified by sequencing. ClpB was overexpressed from the pET28b (+) vector in BL21 (DE3) cells. Six liters of LB media with 30 $\mu g\ mL^{-1}$ kanamycin was used for cell culture at 37°C. The overexpression was induced with 0.5 m*M* isopropyl β-D−1-thiogalactopyranoside (IPTG) at $OD_{600} = 0.8$. After induction the cells were allowed to grow three more hours at 37°C to reach $OD_{600} = 2$. A 23-g cell paste was harvested.

The cell paste was suspended in 100 mL of buffer containing 2 m*M* 2-mercaptoethanol, 40 m*M* Tris (pH 7.5), 500 m*M* NaCl, 20 m*M* imidazole, 20% (v/v) glycerol, and 10% (w/v) sucrose at 4°C. Cells were then lysed with an Ultrasonic liquid processor (Misonix®, USA) and the sample was subjected to centrifugation at 10,500 rpm for 2 h in an SLA-3000 rotor to pellet the cell debris.

The supernatant was loaded onto five 5 mL HisTrap FF™ crude (GE Healthcare) columns equilibrated with Buffer B supplemented with 500 m*M* NaCl and 20 m*M*

imidazole. The column was washed with Buffer B supplemented with 20 m*M* imidazole for 30 column volumes. The sample was eluted with Buffer B supplemented with 500 m*M* NaCl and 500 m*M* imidazole. The fractions from the elution peak were pooled and dialyzed using 15,000 Da molecular weight cut off dialysis tubing against thrombin cleavage buffer (Buffer B supplemented with 300 m*M* NaCl and 3 m*M* $CaCl_2$) overnight and then treated by 1-U thrombin per milligram ClpB for 12 h at 4°C in the same dialysis bag against fresh thrombin cleavage buffer. The sample was then switched to a 50,000 Da cut off dialysis bag to remove the thrombin from the reaction and dialyzed against Buffer B supplemented with 500 m*M* NaCl and 20 m*M* imidazole for 6 h at 4°C.

The dialyzed sample was loaded on the HisTrap FF^{TM} (GE Healthcare) column equilibrated with Buffer B supplemented with 500 m*M* NaCl. The flow through was then dialyzed against Buffer B supplemented with 80 m*M* NaCl. The sample was loaded onto a Heparin Sepharose FF (GE Healthcare) column that was equilibrated with Buffer B supplemented with 80 m*M* NaCl. The column was washed with Buffer B supplemented with 80 m*M* NaCl for two column volumes and then the protein was eluted with Buffer B supplemented with 1*M* NaCl. The fractions containing ClpB were loaded onto Sephacryl S-300 high resolution (GE Healthcare) column that was equilibrated in Buffer B supplemented with 1*M* NaCl. The ClpB fractions were pooled and dialyzed against Buffer B supplemented with 1 *M* NaCl and 50% (v/v) glycerol for storage at −80°C.

The resultant protein was >95% pure as judged by Coomasie staining and its molecular weight was determined by MALDI-TOF mass spectrometry. One species with a molecular weight of 95,817 Da was observed. This result is consistent with the molecular weight of the monomer of ClpB plus two additional amino acids at the N-terminus after removing the His-tag. From 23-g cell paste 600 mg of >95% pure ClpB was acquired using this protocol.

The concentration of ClpB was determined spectrophotometrically from the absorption spectra of several aliquots of ClpB in 6*M* guanidine-HCl. The extinction coefficient in 6*M* guanidine-HCl was calculated from the extinction coefficients of the individual aromatic amino acids in 6*M* guanidine-HCl using Sednterp[25,26] (David Hayes, Magdalen College, Tom Laue, University of New Hampshire, and John Philo, Alliance Protein Laboratories).[27] The extinction coefficient of ClpB in Buffer H was determined by comparing the absorption spectra of three aliquots of ClpB protein in 6*M* guanidine-HCl with the absorption spectra of aliquots of native ClpB in Buffer H supplemented with different NaCl concentrations.

The determined extinction coefficients for ClpB at 280 and 230 nm was found to be $\varepsilon_{280} = (3.6 \pm 0.1) \times 10^4$ (M monomer)$^{-1}$ cm^{-1} and $\varepsilon_{230} = (3.5 \pm 0.1) \times 10^5$ (M monomer)$^{-1}$ cm^{-1}. These values represent the average and standard deviation of 10 replicates collected in the presence of 100, 200, and 300 m*M* NaCl and various protein concentrations. Because ClpB resides in a mixture of oligomers at these three different salt concentrations and protein concentrations (see Results section) and the standard deviation on the extinction coefficient is < 3%, we conclude that there is little detectable difference in the extinction coefficient for each oligomer.

Analytical ultracentrifugation

Analytical ultracentrifugation experiments on ClpB were performed using a Beckman Optima XL-A analytical ultracentrifuge. Sedimentation velocity experiments using absorbance optics were carried out by loading a sample of protein (380 μL) and the protein dialysate (400 μL) into a double sector Epon charcoal-filled centerpiece and subjected to an angular velocity of 40,000 rpm. Absorbance as a function of radial position was collected by scanning the sample cells at a wavelength of 230 or 280 nm as indicated in the text with a radial step-size of 0.003 cm. Absorbance scans were collected every 4 min.

The sedimentation velocity experiment on 10% glycerol was performed by using a Beckman ProteomeLab XL-I analytical ultracentrifuge. The sedimentation velocity experiments using interference optics were carried out by loading a sample of 10% glycerol (425 μL) and water reference (430 μL) into a double sector Epoxy charcoal-filled meniscus matching centerpiece. An angular velocity of 40,000 rpm was used to perform the sedimentation velocity experiments. Interference scans were collected every 30 s at 25°C.

Sedimentation equilibrium experiments were performed by loading a sample of protein (110 μL) and the protein dialysate (120 μL) into a six-sector Epon charcoal-filled centerpiece. Samples were spun at the velocity indicated in the text until sedimentation equilibrium was achieved as judged by WinMatch (David Yphantis, University of Connecticut, Jeff Lary, National Analytical Ultracentrifugation Center, and Storrs, CT).

Analysis of sedimentation velocity data

Sedimentation velocity boundaries were analyzed using SedFit[28] version.14 (Peter Schuck, NIH), where the c(s) analysis was applied by modeling the sedimentation boundaries as solutions of the Lamm equation for noninteracting species.[29] The sedimentation velocity data were checked for errors in the timestamp automatically by V.14 SedFit and no timestamp errors were found.[30,31] The sedimentation coefficient, *s*, is given by Svedberg's equation, as shown in Eq. (1)[32]:

$$s = \frac{M(1-\bar{\nu}\rho)}{Nf} = \frac{MD(1-\bar{\nu}\rho)}{RT} \quad (1)$$

where M is the molecular weight, $\bar{\nu}$ is the partial specific volume of the macromolecule, ρ is the density of the buffer, R is the ideal gas constant, T is absolute temperature in Kelvin, N is Avogadro's number, f is the frictional coefficient, and D is the diffusion coefficient.

The weight average sedimentation coefficient was calculated from the c(s) distribution by integrating over the area of the c(s) distribution. All sedimentation coefficients, s, reported in the text if not indicated otherwise are corrected to standard buffer condition, 20°C in water, that is, $s_{20,w}$ using Eq. (2)33:

$$s_{20,w} = \frac{(1-\rho_{20,w}\bar{\nu})}{(1-\rho\bar{\nu})} \cdot \frac{\eta}{\eta_{20,w}} \cdot s \qquad (2)$$

where $\rho_{20,w}$and $\eta_{20,w}$ are the density and viscosity of water at 20°C, respectively. ρ and η are the density and viscosity of buffer at the experimental temperature, respectively.

Analysis of sedimentation equilibrium data

Sedimentation equilibrium boundaries were subjected to global nonlinear-least-squares (NLLS) fitting using HeteroAnalysis (James L. Cole and Jeffrey W. Lary, Storrs CT) and the single ideal species model provided in the software.[34,35] The partial specific volume for ClpB, $\bar{\nu} = 0.7403$ mL g^{-1}, was calculated from the primary sequence. Because these experiments were performed in the presence of 10% glycerol, the partial specific volume was corrected using Eq. (3) as reported by Cole[35] and previously applied to the examination of ClpA[36] by us, which accounts for the changes in hydration due to the presence of the glycerol.

$$\frac{\Delta\bar{\nu}}{\Delta[\text{glycerol}]\%(\text{v/v})} = (3.33 \pm 0.38) \times 10^{-4} \text{mL g}^{-1} \qquad (3)$$

Taking into account the 10% glycerol used in our experiments results in a correction of $\Delta\bar{\nu} = +0.0033$ mL g^{-1}, which gives a partial specific volume for ClpB in 10% glycerol of $\bar{\nu} = 0.7436$ mL g^{-1}. The density of the buffer was calculated from the buffer components using Sednterp.[25] The density of buffer and partial specific volume of ClpB were set as 1.03253 g mL^{-1} and 0.7436 mL g^{-1} in the "options" tab in HeteroAnalysis, respectively.

Sedimentation coefficients (s) estimation from global fitting of the time difference curves

Sedimentation coefficients, s, for ClpB monomers and hexamers were determined experimentally. Sedimentation coefficients for other ClpB oligomers were calculated using WinHydroPRO.[37] This was accomplished using a simulated *E. coli* ClpB hexamer structure based on the monomer crystal structure, which was kindly provided by Dr. Rebecca Wade.[16,38] ClpB dimer, trimer, tetramer, and pentamer model structures were generated using VMD[39] by removing four, three, two, or one adjacent protomers, respectively from the hexameric ring model. Thus, the interface between ClpB protomers for these oligomers was preserved to be the same as in the ClpB hexamer model. For the dimer, trimer, tetramer, and pentamer the "shell model from residual-level" model was used for calculation as recommended by A. Ortega *et al.*[37] The sedimentation coefficients for ClpB oligomers in buffer H supplemented with 100, 200, and 300 mM NaCl based on this calculation are constrained in the global fitting of the time difference curves to the values presented in Table I for the various models tested.

Table I
Sedimentation Coefficients for ClpB Oligomers Used in Global Analysis of Sedimentation Velocity Data

1-2-4-6	Monomer	Dimer	Trimer	Tetramer	Pentamer	Hexamer
M.W. (Da)	95,817	191,634	287,451	383,268	479,085	574,902
100 m*M* NaCl	3.6	5.88	7.73	9.30	11.08	12.5
200 m*M* NaCl	3.07	5.65	7.42	8.93	10.64	12.2
300 m*M* NaCl	3.00	5.6	7.36	8.86	10.56	11.9

The sedimentation coefficients used in the analysis are not corrected to$s_{20,w}$, the values presented in this table have units of S (Svedberg), as 10^{-13} s.

The sedimentation coefficients were also calculated using Eq. (4) with the assumption that ClpB monomer and n-mer have the same frictional ratio.[33]

$$s_n = s_1 (n)^{\frac{2}{3}} \qquad (4)$$

However, the calculated s_6 is 6% different from the experimental value when applying the experimentally determined s_1 to Eq. (4). On the other hand, s_6 predicted using HydroPro is only 2% different from the experimental value determined for the hexamer. Moreover, fits by allowing s values for the intermediates to float within the value range predicted by Eq. (4) and HydroPro show that changes in the sedimentation coefficient that fall within the bounds predicted by Eq. (4) and HydroPro have no significant impact on the determined equilibrium constants (fitting not shown).

Global fitting of sedimentation velocity data using the time difference curve method

SedAnal[40] was used to globally fit sedimentation velocity data at various ClpB concentrations to obtain thermodynamic and, if present, kinetic information on ClpB assembly. SedAnal calculates and fits the time difference curves. The data were examined by two different strategies in an effort to rule out models that do not adequately describe the experimental observations. In

summary, the first strategy solves the path independent equilibrium equations and no information on kinetic rate constants is obtained. The second strategy solves the system of coupled differential equations describing the kinetics and therefore, under limiting conditions, can yield information on the kinetic rate constants. Specifically, the dissociation rate constants are used as the fitting parameters. It is important to note that since the system of coupled differential equations are being solved for a specific mechanism the rate constants determined are elementary rate constants and not observed rate constants or relaxation times, where both the observed rate constant and the relaxation time are composites of several elementary rate constants. For a detailed description of how this was accomplished see Lin and Lucius, Methods in Enzymology, in press.

Throughout the manuscript, the following notation is used to describe reaction schemes. The reactions given by Eqs. (6)–(8) are noted as "1–2, 1–4, 1–6" to indicate stoichiometric assembly reactions. Whereas, Eqs. (9)–(11) are denoted as 1–2–4–6 to indicate step-wise assembly reactions.

Sedimentation coefficients, molecular weights, density increment, and extinction coefficient were all constrained in the analysis. The extinction coefficients for ClpB ($\times$ 1.2 cm path length) used in the global fitting are (0.45 ± 0.01) mL mg^{-1} at 280 nm and (4.4 ± 0.1) mL mg^{-1} at 230 nm. The protein loading concentrations, dissociation rate constants, and association equilibrium constants were floated as indicated in the models.

For each final set of parameters presented here, the Nonlinear-Least-Squares fit (NLLS) was performed multiple times by starting with different initial guesses for the parameters. This was done to insure that the examination resulted in the same set of parameters regardless of starting point. Moreover, this strategy provides evidence that the results are not the consequence of local minima.

F-test was used to compare the goodness of fits between two models applied to the same experimental data set. $F_{\text{calculated}}$ is calculated using Eq. (5) [derived from Johnson & Straume Eq. (45)],[41]

$$F_{\text{calculated}} = \frac{RMSD_1^2}{RMSD_2^2} \tag{5}$$

where RMSD_1 and RMSD_2 are the root mean squared deviation for the two fits being compared. RMSD_1 is always chosen to be equal to or greater than RMSD_2, so that the $F_{\text{calculated}}$ is always larger than unity. $F_{\text{calculated}}$ is compared to F_{critical}, where F_{critical} was determined using the "F-calculator" that is embedded in SedAnal.[41] If $F_{\text{calculated}}$ is greater than F_{critical}, the two fits are statistically different and the fit with the smaller RMSD can be concluded to be a significantly better fit.

To determine the error space on the resulting fitting parameters, "Johnson & Straume Eq. (35)"[41] was used to calculate the confidence intervals for each parameter by selecting the "F-statistics" function that is built into SedAnal. That is to say, to determine the errors for each parameter, *F*-test was also performed by clicking "Calculate F-statistics" in "advance" setting. In addition, the F_{critical} value used to determine the maximum and minimum values for each parameter was calculated using Johnson & Straume Eq. (35).[41] The confidence level for the uncertainty on each parameter was set at 68.3%.

RESULTS

ClpB exhibits dynamic assembly in the absence of nucleotide

To quantitatively examine the ClpB association mechanism, we performed sedimentation velocity experiments at multiple ClpB concentrations ranging from 1 to 15 μM in buffer H supplemented with 300 mM NaCl. Figure 1(a) shows a series of absorbance boundaries collected with 6 μM ClpB by monitoring absorbance at 280 nm as a function of radial position and time. The data were subjected to c(s) analysis using SedFit (Peter Shuck, NIH) and the red solid lines in Figure 1(a) represent the fit. The residuals from the analysis are shown in Figure 1(b); they are randomly distributed about zero and, on average, <0.01 absorbance units, indicating that the fit describes the data well.

Figure 1(c) shows the c(s) distribution obtained from analyzing the raw data from sedimentation velocity experiments performed with 6 μM (red), 9 μM (blue), and 15 μM (green) ClpB. At 6 μM ClpB, two broad c(s) distributions are observed and a weighted average sedimentation coefficient, $\bar{s}_{20,w} = (7.2 \pm 0.4)$ S was determined [see red trace in Fig. 1(c)], where the uncertainty represents the standard deviation determined from three independent measurements. At a ClpB concentration of 9 μM, $s_{20,w}$ increased to (9.0 ± 0.4) S indicating that larger oligomers form at this higher ClpB concentration. The c(s) distribution continues to shift to higher sedimentation coefficient values as the concentration of ClpB is elevated to 15 μM [see green traces in Fig. 1(c)].

In Figure 1(c) the distribution around 5 S appears to shift to larger sedimentation coefficient values with increasing protein concentration. This observation suggests that one or more than one ClpB oligomer may exhibit rapid dissociation on the time scale of sedimentation.[42] Hence, the c(s) distributions may represent reaction boundaries of ClpB oligomers and the peaks are not likely representative of discrete species. Consequently, we sought to find conditions where we could perturb the equilibrium in a way that would favor discrete species.

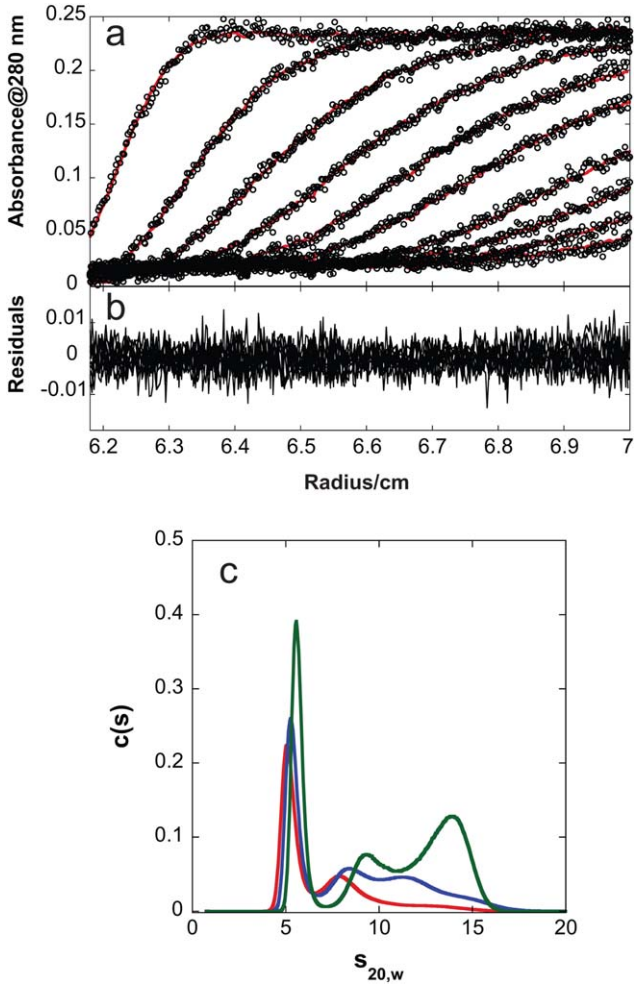

Figure 1

ClpB exhibits dynamic assembly in the absence of nucleotide. (**a**) Raw sedimentation velocity scans as function of radial position for 6 μM ClpB in buffer H300 at 25°C. The scans were collected every 4 min at 280 nm, every 8th scan is shown. Open circles are data and red solid lines are fits generated from c(s) analysis; (**b**) Residuals of fit. (**c**) c(s) distribution for ClpB assembly in buffer H supplemented with 300 m*M* NaCl at 6 (red), 9 (blue), and 15 (green) μM ClpB monomer. [Color figure can be viewed in the online issue, which is available at wileyonlinelibrary.com.]

NaCl concentration has a strong impact on ClpB assembly

Schlee *et al.* reported that decreasing the salt concentration drives ClpB to form large oligomers.[17,43] Therefore, we performed sedimentation velocity experiments to examine the impact of [NaCl] on the distribution of states. Sedimentation velocity experiments with 2 μM ClpB in buffer H at 300, 200, and 100 m*M* NaCl were performed as described in Materials and Methods. The data were subjected to c(s) analysis and the c(s) distribution for ClpB at each [NaCl] is shown in Figure 2(a–c).

For 2 μM ClpB at 300 m*M* NaCl, the c(s) distribution shows one predominant peak with an $s_{20,w} = (5 \pm 1)$ S,

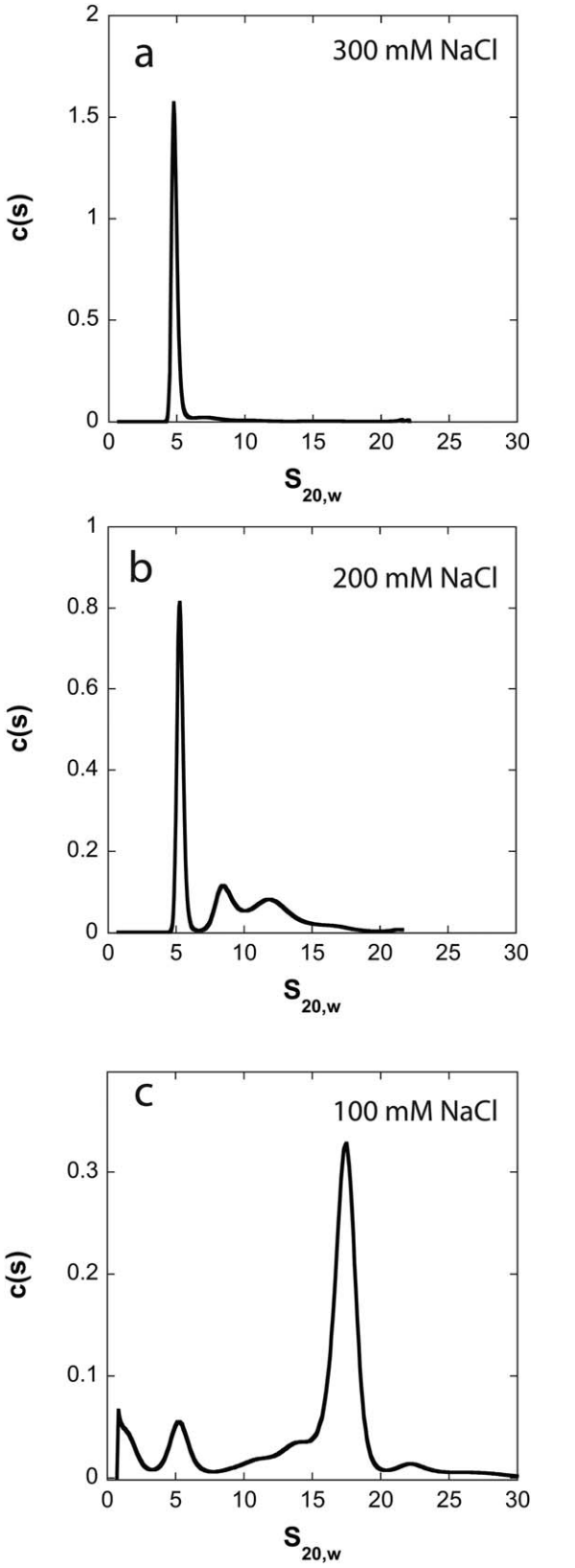

Figure 2

Salt effect on ClpB assembly. The c(s) distribution versus $s_{20,w}$ for 6 μM ClpB in Buffer H with NaCl concentration indicated in panel a, b, and c.

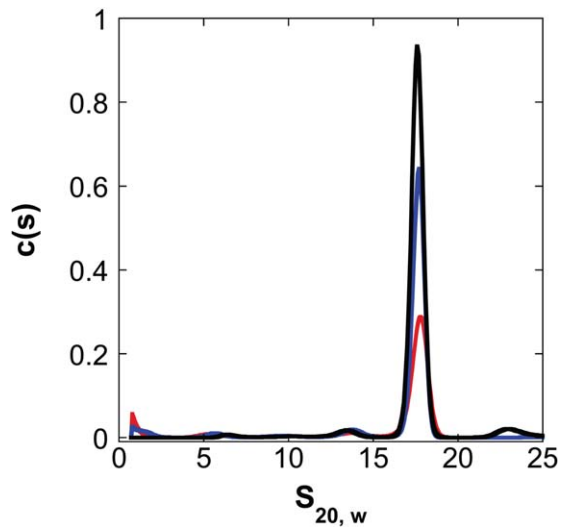

Figure 3

One ClpB oligomer is predominately populated in 100 m*M* NaCl. The c(s) distribution versus $s_{20,w}$ of 6 (red), 9 (blue) and 15 (black) μ*M* ClpB in Buffer H with 100 m*M* NaCl at 25°C. [Color figure can be viewed in the online issue, which is available at wileyonlinelibrary.com.]

where the uncertainty is determined from the analysis performed in SedFit. Figure 2(b) shows that decreasing the [NaCl] to 200 m*M* results in a shift to the right and a broad distribution is observed with sedimentation coefficients ranging from 4.4 S to 18.6 S. Consistently, as the [NaCl] is further decreased to 100 m*M* the distribution shifts farther to the right [see Fig. 2(c)]. Noticeably, under these conditions, one major peak at (17.6 ± 0.6) S begins to emerge. This ~17.6 S distribution peak didn't shift significantly to larger $s_{20,w}$ values when the [NaCl] was decreased further to 50 m*M* (data not shown).

One ClpB oligomer is predominately populated at 100 mM NaCl

We next examined the ClpB concentration dependence of the assembly reaction at 100 m*M* NaCl since it appears as though a single ClpB oligomer is emerging at low NaCl concentrations. Sedimentation velocity experiments in buffer H supplemented with 100 m*M* NaCl were performed at various ClpB concentrations ranging from 4 to 18 μM. Strikingly, one predominate c(s) peak was observed at all examined ClpB concentrations (see Fig. 3). Increasing the ClpB concentration didn't shift the (17.6 ± 0.6) S c(s) peak indicating that this peak likely represents the largest ClpB oligomer that is significantly populated in the 100 m*M* NaCl conditions.

In Figure 3, for 15 μ*M* ClpB, the emergence of a minor distribution is observed centered about an $s_{20,w}$ = (23 ± 2) S. This could represent a reaction boundary for a larger oligomer. However, the peak area doesn't appear to have a clear ClpB concentration dependence, which suggests those oligomers, if present, may exhibit weak assembly and their population is not sufficiently large to be accurately determined at these [ClpB]. This is further indicated by the fact that the observed peak area of the 23 S peak is <5% of the entire c(s) distribution.

Determination of the molecular weight of the largely populated ClpB oligomer in the absence of nucleotide in buffer H with 100 mM NaCl

To determine the molecular weight of the ClpB oligomer that we report here to have $s_{20,w}$ = (17.6 ± 0.6) S, we performed sedimentation equilibrium experiments with 4, 6, 9, 12, 15, and 18 μ*M* ClpB in buffer H with 100 m*M* NaCl at 25°C. The sedimentation equilibrium data as a function of radial position and [ClpB] are shown in Figure 4. The data were globally analyzed using the "single ideal species" model in HeteroAnalysis(James Cole and Jeffery Lary).[34] The molecular weight of the single species was allowed to float as the fitting parameter and the determined molecular weight, *M* = (578 ± 3) kDa is in good agreement with the value calculated from the primary structure of ClpB as a hexamer of 575 kDa. The fitting root mean squared deviation (RMSD) is 0.0090 indicating the data are well described by this model. This is consistent with the analysis of the sedimentation velocity data shown in Figure 3.

To examine the precision in the determination of the hexamer, we asked the question; can the sedimentation equilibrium data be equally well described if the predominant oligomer is assumed to be a pentamer or heptamer? Although there has been no report concluding ClpB forms pentamers, the question here is; could our determination of the molecular weight be off by plus or minus one protomer unit? To address this question, we constrained the molecular weight to be either 479 or 671 kDa, the molecular weight of the pentamer or heptamer, respectively. In this analysis, the partial specific volume was $\bar{\nu} = 0.7436$ mL mg^{-1}, which is corrected for the presence of 10% glycerol (see Materials and Methods). The analysis resulted in an RMSD = 0.0131 assuming a pentamer and an RMSD = 0.0120 assuming a heptamer. Comparing to the RMSD = 0.0090 where the molecular weight is allowed to float and determined to be *M* = (578 ± 3) kDa, the analyses assuming pentamer or heptamer are both significantly worse.

An alternate way in which the determined molecular weight could be off by as much as one promoter unit would be if the error in the partial specific volume is sufficiently large. The experiments performed here have been carried out in 10% glycerol, which can lead to a dynamic gradient of glycerol. This could lead to

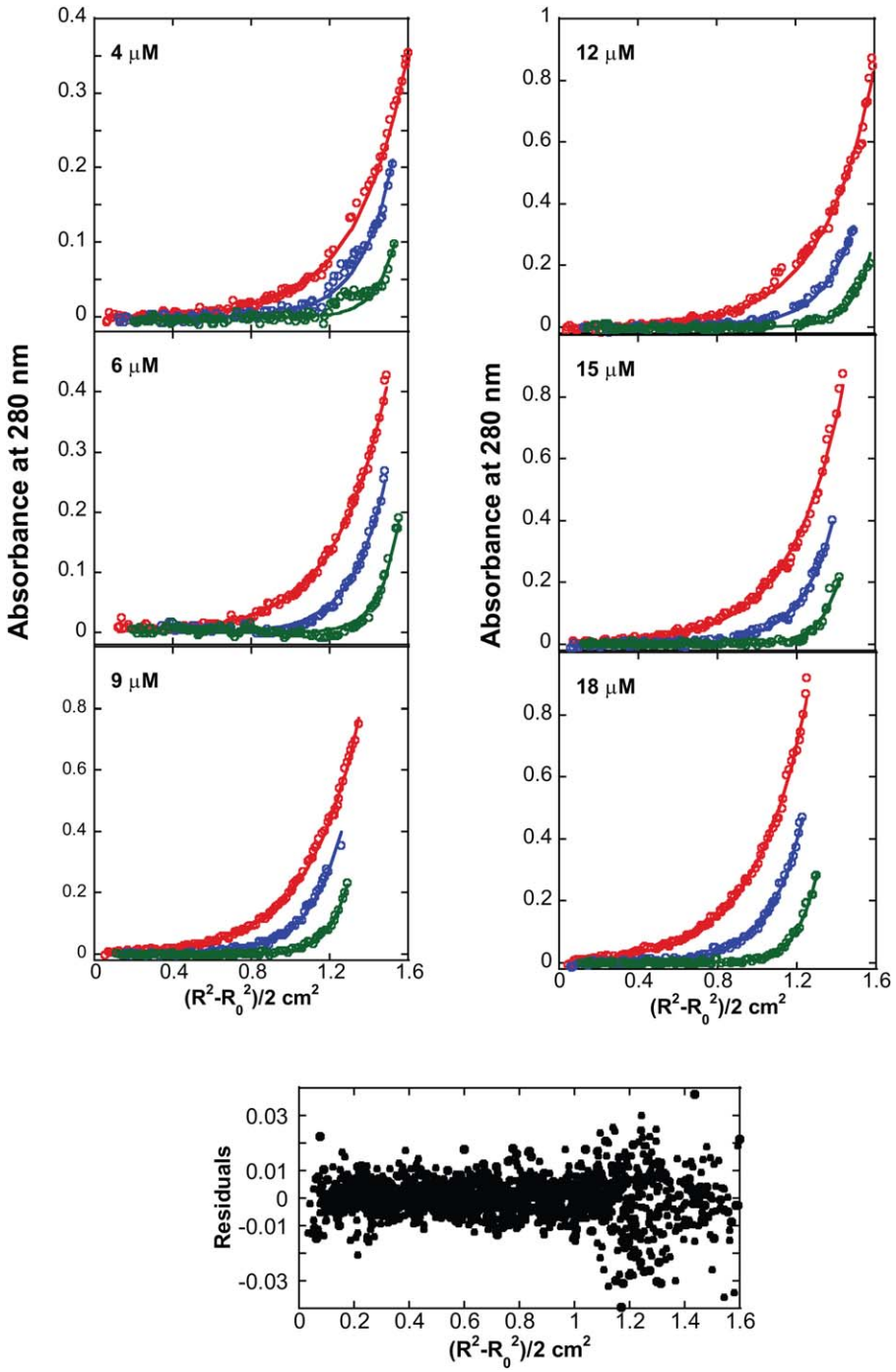

Figure 4

Global fitting of sedimentation equilibrium scans. Scans were collected with 4, 6, 9, 12, 15, and 18 μ*M* ClpB, in 100 m*M* NaCl at 25°C, at 8,000 (red), 10,000 (blue), and 13,000 (green) rpm. The radial position is presented as $(R^2 - R_0^2)/2$, where R is the radial position of each absorbance datum and R_0 is the radial positon of the meniscus of the sample. The data were subjected to NLLS analysis using Heteroanalysis using the single ideal species model. The open circles are the raw data and the solid lines are the fits. The residuals from the fits are shown in filled circles. The resulting molecular weight from the analysis is (578 ± 3) kDa. The fitting RMSD is 0.0090 ± 0.0003. [Color figure can be viewed in the online issue, which is available at wileyonlinelibrary.com.]

uncertainty in the partial specific volume. However, we have performed an extensive analysis of the impact of the inclusion of the 10% glycerol and conclude that it does not impact the determined parameters, see Supporting Information Figures S1, S2 and the corresponding presentation.

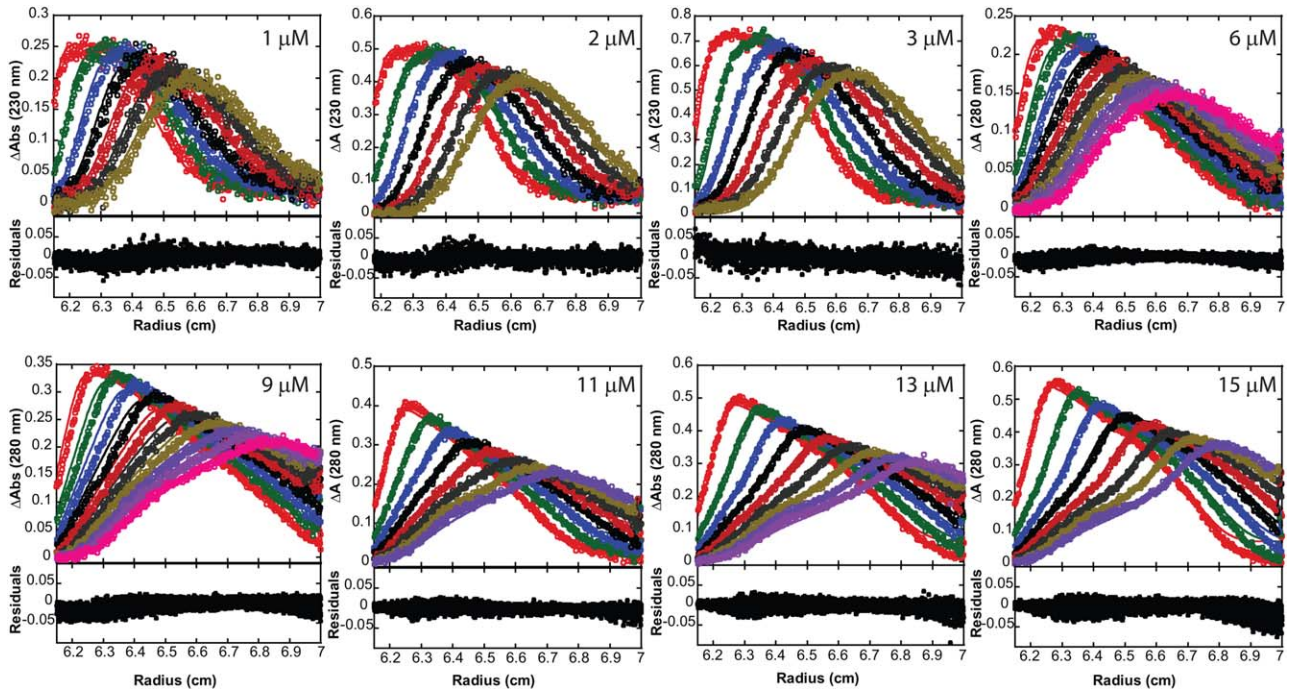

Figure 5

Time difference curves from Sedimentation velocity experiments performed on multiple ClpB concentrations in the presence of 300 m*M* NaCl. The loading concentrations of ClpB are indicated on the plots. For each ClpB concentration, the ΔAbsorbance time differences curves as a function of radial position are shown in the top panel and the residuals from the fit are shown in the bottom panel. The open circles are the raw data and the solid lines are the fit to the 1–2–4–6 model. The resultant parameters and RMSD are given in Tables III and IV. [Color figure can be viewed in the online issue, which is available at wileyonlinelibrary.com.]

Determination of the assembly model for ClpB

From sedimentation equilibrium experiments presented in Figure 4, we conclude the 17.6 S species is hexameric ClpB. In comparison to the c(s) distribution determined in the presence of 100 m*M* NaCl, the c(s) distribution for ClpB in the presence of 300 m*M* NaCl did not exhibit a significant distribution at ∼17.6 S [cf., Figure 2(a) to (c)]. Rather, in the presence of 300 m*M* NaCl a broad c(s) distribution as a function of ClpB concentration was detected and the apparent c(s) peak positions do not superimpose [see Fig. 1(c)]. This indicates that ClpB oligomers may exhibit rapid dissociation on the time scale of sedimentation. Alternatively, oligomers between monomers and hexamers may be present.

To resolve these possibilities we globally analyzed the data using the time difference curve method (see Materials and Methods).[40] Shown in Figure 5 are the difference curves for sedimentation velocity experiments collected with 1, 2, 3, 6, 9, 11, 13, and 15 μM ClpB in Buffer H with 300 m*M* NaCl. These data were subjected to global NLLS analysis with the simplest monomer to hexamer model. This model assumes that only monomers and hexamers are significantly populated at thermodynamic equilibrium. However, it is important to note that this model does not rule out the possibility that intermediates are present. If the model adequately describes the data it only allows for the conclusion that intermediates are not sufficiently populated to be detected in the analysis. Nevertheless, the data are not well described by this model with an RMSD = 3.374×10^{-2} (fit not shown). Thus, we conclude that at least one intermediate must be significantly populated.

Because monomers and hexamers may be present, we globally analyzed the difference curves in Figure 5 with the assumption that at least monomers and hexamers are present and one intermediate is also present. The RMSD values for the analysis including a dimeric, trimeric, or tetrameric intermediate are given in Table II. All of these "three species" models do not adequately describe the sedimentation boundaries as judged by comparing the RMSDs using *F*-test (Table II).

It is possible that the hexamer may not be significantly populated at the elevated salt concentration of 300 m*M* NaCl. Thus, we analyzed the data with a monomer–dimer, monomer–tetramer model ("1–2, 1–4" model in Table II). Based on the RMSD this model also did not adequately describe the experimental observations (see Table II).

Table II shows that the data are not adequately described by a two species (1–6) or any of the three

Table II
Model Determination for ClpB Assembly in Buffer H with 300 m*M* NaCl

Model	RMSD	$F_{calculated}$
1–6	3.374×10^{-2}	11.686
1–2, 1–6	1.055×10^{-2}	1.143
1–3, 1–6	1.201×10^{-2}	1.481
1–4, 1–6	1.672×10^{-2}	2.870
1–2, 1–4	1.748×10^{-2}	3.137
1–2, 1–3, 1–6	0.999×10^{-2}	1.024
1–2, 1–4, 1–6	0.987×10^{-2}	1
Isodesmic	2.172×10^{-2}	4.843

All models in the table represent stoichiometric binding reactions, for example, 1–6 indicates monomers forming hexamers. An $F_{calculated}$ value larger than an $F_{critical}$ value = 1.005 indicates a significantly worse fit compared to the best fit. The "1–2, 1–4, 1–6" fit is significantly better than any other fit presented in this table. Thus, all other models were compared to this model. $F_{calculated}$ was determined as described in materials and methods. The value of $F_{calculated} = 1$ indicates the model that best describes the data.

species models ("1–2, 1–6", etc). These observations may suggest that there are more intermediates present at thermodynamic equilibrium. To test this possibility, we analyzed the data with the "1–2, 1–3, 1–6" or the "1–2, 1–4, 1–6" models. Both of these models describe the data well. However, the "1–2, 1–4, 1–6" model describes the data significantly better based on the RMSD and the *F*-tests shown in Table II.

The data can be well described by including monomers, dimers, tetramers, and hexamers. However, an energetically simpler model is the isodesmic model because it assumes all the equilibrium constants are the same even though it includes every intermediate from monomers to hexamers. As shown in Table II, the isodesmic model does not describe the data as well as either the "1–2, 1–3, 1–6" or the "1–2, 1–4, 1–6" model. Moreover, the "1–2, 1–4, 1–6" model yields the lowest RMSD.

Determination of the assembly path for ClpB

To test if the sedimentation velocity experiments reported here are sensitive to the kinetics of dissociation, the difference curves in Figure 5 were subjected to global NLLS analysis by modeling the reaction kinetics as described in Materials and Methods. However, analysis of these data by incorporating rate constants for each of the steps results in the model no longer being path-independent as assumed when modeling for only the equilibrium constants. Consequently, the first step in this analysis strategy is to determine the path that best describes the data.

There are many paths for ClpB monomers to form hexamers. However, the probability of three bodies colliding in a single kinetic step is diminishingly small. Thus, we sought to describe the data with the simplest model that requires each oligomer to form through bimolecular interactions. The analysis of the sedimentation velocity data shown in Figure 5 was best described by the "1–2, 1–4, 1–6" path-independent stoichiometric model given by the reactions in Eqs. (6)–(8).

$$2B_1 \overset{L_{2,0}}{\rightleftharpoons} B_2 \tag{6}$$

$$4B_1 \overset{L_{4,0}}{\rightleftharpoons} B_4 \tag{7}$$

$$6B_1 \overset{L_{6,0}}{\rightleftharpoons} B_6 \tag{8}$$

To transition to incorporating the kinetics into this model we subjected the difference curves to analysis using the step-wise 1–2–4–6 model given by the reactions in Eqs. (9)–(11).

$$2B_1 \overset{K_2}{\rightleftharpoons} B_2 \tag{9}$$

$$2B_2 \overset{K_4}{\rightleftharpoons} B_4 \tag{10}$$

$$B_2 + B_4 \overset{K_6}{\rightleftharpoons} B_6 \tag{11}$$

Figure 5 shows a representative set of difference curves and global NLLS fit using the 1–2–4–6 model. The resultant step-wise equilibrium constants, K_n, are given in Table III and the resultant reverse rate constants, $k_{r,n}$, are given in Table IV both under the heading of 300 m*M* NaCl. Table III also reports the stoichiometric binding constants, $L_{n,0}$ that were calculated using the relationships given by Eqs. (12)–(14).

$$L_{2,0} = K_2 \tag{12}$$

$$L_{4,0} = K_2^2 \cdot K_4 \tag{13}$$

$$L_{6,0} = K_2^3 \cdot K_4 \cdot K_6 \tag{14}$$

The analysis of the difference curves shown in Figure 5 yielded dissociation rate constants that floated to values larger than 0.01 s^{-1} (see Table IV for 300 mM NaCl). If all the reactions given by Eqs. (9)–(11) have reverse rate constants, $k_r > 0.01\ s^{-1}$ then the data should be equally well described by stoichiometric equilibrium constants given by Eqs. (15)–(17) (Lin and Lucius, Methods in Enzymology manuscript in press).

$$K_2 = \frac{k_{f2}}{k_{r2}} = \frac{[B_2]}{[B_1]^2} \tag{15}$$

$$K_4 = \frac{k_{f4}}{k_{r4}} = \frac{[B_4]}{[B_2]^2} \tag{16}$$

$$K_6 = \frac{k_{f6}}{k_{r6}} = \frac{[B_6]}{[B_2][B_4]} \tag{17}$$

In other words, the difference curves should not contain any information on path. Thus, a model using step-wise equilibrium constants, K_n, (1–2–4–6 model) or a

Table III
Global Fitting Results of Sedimentation Velocity Experimental Data at Multiple ClpB Concentrations in Buffer H with the NaCl Concentration Indicated in the Table

	300 m*M* NaCl		200 m*M* NaCl		100 m*M* NaCl	
	RMSD = 9.01×10^{-3}		RMSD = 7.65×10^{-3}		RMSD = 9.65×10^{-3}	
Reactions (1–2–4–6 model)	K_n (M^{-1})	Calculated $L_{n,0}$	K_n (M^{-1})	Calculated $L_{n,0}$	K_n (M^{-1})	Calculated $L_{n,0}$
$2B \rightleftharpoons B_2$	8.9 (8.8, 9.0) $\times 10^4$	8.9 (8.8, 9.0) $\times 10^4$	1.73 (1.68, 1.78) $\times 10^5$	1.73 (1.68, 1.78) $\times 10^5$	9.5 (6.0, 18.6) $\times 10^4$	9.5 (6.0, 18.6) $\times 10^4$
$2B_2 \rightleftharpoons B_4$	1.83 (1.75, 1.92) $\times 10^5$	1.44 (1.36, 1.52) $\times 10^{15}$	1.9 (1.8, 2.0) $\times 10^6$	5.8 (5.4, 6.2) $\times 10^{16}$	4.2 (1.0, 11.9) $\times 10^8$	3.8 (−0.2, 13.9) $\times 10^{18}$
$B_2 + B_4 \rightleftharpoons B_6$	8.6 (8.4, 8.9) $\times 10^5$	1.10 (1.03, 1.17) $\times 10^{26}$	2.0 (1.9, 2.1) $\times 10^7$	2.0 (1.8, 2.2) $\times 10^{29}$	1.6 (1.0, 2.3) $\times 10^9$	5.8 (−2.2, 26) $\times 10^{32}$
Reactions (1–2, 1–4,	RMSD = 9.87×10^{-3}		RMSD = 8.02×10^{-3}		RMSD = 9.97×10^{-3}	
1–6 model)	Calculated K_i (M^{-1})	$L_{n,0}$	Calculated K_i (M^{-1})	$L_{n,0}$	Calculated K_i (M^{-1})	$L_{n,0}$
$2B \rightleftharpoons B_2$	9.7 (9.5, 9.8) $\times 10^4$	9.7 (9.5, 9.8) $\times 10^4$	1.47 (1.41, 1.52) $\times 10^5$	1.47 (1.41, 1.52) $\times 10^5$	0 (0, 7.8) $\times 10^3$	0 (0, 7.8) $\times 10^3$
$4B \rightleftharpoons B_4$	1.6 (1.5, 1.7) $\times 10^5$	1.5 (1.4, 1.6) $\times 10^{15}$	2.0 (1.8, 2.2) $\times 10^6$	4.4 (4.2, 4.6) $\times 10^{16}$	NA	0.9 (0.6, 1.1) $\times 10^{18}$
$6B \rightleftharpoons B_6$	9 (8, 10) $\times 10^5$	1.34 (1.31, 1.37) $\times 10^{26}$	2.9 (2.7, 3.1) $\times 10^7$	1.89 (1.84, 1.95) $\times 10^{29}$	NA	3.9 (3.5, 4.2) $\times 10^{32}$

Note: Analysis using the "1–2, 1–4, 1–6" model employed the Newton–Raphson method to determine the concentration of each species by numerically solving the conservation of mass equation given by Eq. (6). Whereas, analysis of data using the 1–2–4–6 employed the kinetic integrator (SEulEx) to numerically solve the system of coupled differential equations for the reactions. The step-wise equilibrium constants, K_n, were used as fitting parameters when the data were examined using the 1–2–4–6 model to describe the data. The stoichiometric equilibrium constants, $L_{n,0}$, were used as fitting parameters when the data were examined using the "1–2, 1–4, 1–6" model. The corresponding equilibrium constant, $L_{n,0}$ or K_n were calculated using Eq. (12)–(14). The data are collected in buffer H with the NaCl concentration indicated in the table. The units on $L_{n,0}$ is $M^{-(n-1)}$.

Table IV
Kinetic Parameters Determined from Global NLLS Analysis that are Associated with 1–2–4–6 Model Presented in Table III

Reactions (1–2–4–6 model)	300 m*M* NaCl RMSD = 9.01×10^{-3} $k_{r,n}$ (s^{-1})	200 m*M* NaCl RMSD = 7.65×10^{-3} $k_{r,n}$ (s^{-1})	100 m*M* NaCl RMSD = 9.65×10^{-3} $k_{r,n}$ (s^{-1})
$2B \underset{k_{r2}}{\overset{k_{f2}}{\rightleftharpoons}} B_2$	4.1*	5.6 (5.1, 6.1) $\times 10^{-3}$	0.2*
$2B_2 \underset{k_{r4}}{\overset{k_{f4}}{\rightleftharpoons}} B_4$	0.01*	6.4*	0.04*
$B_2 + B_4 \underset{k_{r6}}{\overset{k_{f6}}{\rightleftharpoons}} B_6$	0.7*	5.4*	1.3 (1.0, 1.6) $\times 10^{-3}$

Some rate constants floated to values $\geq 0.01\ s^{-1}$ (noted with a "*"), which is outside of the measureable range. Therefore, those rate constants were not allowed to float for F-statistic error determination and the errors for those parameters were not determined.

model using stoichiometric binding constants, $L_{n,0}$ (1–2, 1–4, 1–6) as floating parameters should describe the data equally well. However, as seen in Table III, the 1–2–4–6 model, where the reverse rate constants for each step are floated, describes the data significantly better (based on an *F*-test of the RMSD) than the "1–2, 1–4, 1–6" model, which contains no rate constants.

It is important to note that the 1–2–4–6 model contains three additional floating parameters (three rate constants) compared to the "1–2, 1–4, 1–6" model that does not contain rate constants. However, the three additional parameters are not the reason for the improved RMSD exhibited in Table III for the 300 m*M* NaCl data. The RMSD for the two fits is the sum of the squared residuals divided by the degrees of freedom. The degrees of freedom are defined as the number of data points minus the number of floating parameters. Because the two fits are performed on ~35,000 data points, the addition of three parameters does not significantly change the degrees of freedom. Thus, the improvement in the fit when the rate constants are allowed to float as fitting parameters cannot be dismissed as the simple consequence of three additional fitting parameters. However, we acknowledge that the value of the reverse rate constants for this fit (see Table IV) are not well constrained because they are outside of the expected measurable range of 10^{-2} to $10^{-5}\ s^{-1}$. Nevertheless, constraining these rate constants to the empirical upper limit of $10^{-2}\ s^{-1}$ resulted in a statistically worse fit (data not shown). Consequently, we are forced to conclude that some information on these rate constants must be present in the data.

Table V
Comparison of the Goodness of Fit for Three Replicates to the 1–2–3–6 versus the 1–2–4–6 Model

Replicates	1–2–3–6 $RMSD_1$ of Fit	1–2–4–6 $RMSD_2$ of Fit	$F_{Calculated}$[a] Eq. (5)	F_{table} Confidence level: 68.3%
1	9.95×10^{-2}	9.01×10^{-3}	1.220	1.005
2	1.090×10^{-2}	1.082×10^{-2}	1.015	1.005
3	1.137×10^{-2}	1.111×10^{-2}	1.047	1.005

[a]For the calculation of $F_{Calculated}$, recall, $RMSD_1$ is defined as the larger standard deviation, see Materials and Methods.

With respect to the stoichiometric assembly models, Table II indicates that the "1–2, 1–3, 1–6" model represents the next best model compared to the "1–2, 1–4, 1–6" model. This conclusion is based on the F-statistic presented in Table II. Thus, we asked the question; upon incorporation of path information could a step-wise 1–2–3–6 model describe the experimental observations better than the step-wise 1–2–4–6 model? To address this question we subjected the difference curves in Figure 5 to global NLLS analysis using the step-wise 1–2–3–6 model. Further, two additional replicates of the same concentration-dependent data were analyzed to the 1–2–3–6 and the 1–2–4–6 models and the RMSD values and F-statistics are reported in Table V. In all cases the 1–2–4–6 model describes the data significantly better than the 1–2–3–6 model. Thus, we conclude that the step-wise 1–2–4–6 model represents the best description of the experimental observations.

Global analysis of sedimentation velocity data collected in the presence of 100 and 200 mM NaCl

Sedimentation velocity data collected in the presence of 200 and 100 m*M* NaCl were subjected to global NLLS analysis using the "1–2, 1–4, 1–6" model (no kinetic parameters) and the 1–2–4–6 models (including kinetic parameters). The fitting results, together with the results for buffer H supplemented with 300 m*M* NaCl, are presented in Table III. The kinetic parameters from the analysis to the 1–2–4–6 model are presented in Table IV. The difference curves and the best fits are shown in the Supporting Information as Figure S3 for 200 m*M* NaCl and Supporting Information Figure S4 for 100 m*M* NaCl buffer.

From the analysis of sedimentation velocity experiments in the presence of either 200 m*M* NaCl or 100 m*M* NaCl with the 1–2–4–6 model and floating the step-wise equilibrium constants, K_n, and reverse rate constants, $k_{r,n}$, we find that most of the rate constants are at or above the empirical boundary for instantaneous dissociation ($10^{-2}\ s^{-1}$). However, the dissociation rate constant for hexamer formation, in the presence of 100 m*M* NaCl, is within the measureable range (see Table IV for rate constants). In all cases, based on the fitting RMSD and subsequent *F*-test, the data are better described by the step-wise 1–2–4–6 model compared to the "1–2, 1–4, 1–6" model.

For comparison purposes, the stoichiometric binding constant was calculated when fitting to the 1–2–4–6 model and the step-wise constant was calculated when

fitting to the "1–2, 1–4, 1–6" model using the relationships in Eqs. (12)–(14), see Table III. Although the RMSD is better in all cases when fitting using the 1–2–4–6 model compared to the "1–2, 1–4, 1–6" model the parameters are similar. However, in most cases, the parameters are slightly outside of the uncertainty calculated using the F-statistics (see Table III).

It is important to note that the uncertainties reported on the parameters in Table III are from the F-statistic function built into Sedanal and represent fitting error. The uncertainty that would represent the reproducibility is likely larger. To quantify this assertion we present the average of three experimental replicates of the entire protein concentration range collected in the presence of 300 m*M* NaCl and subsequent fits. Supporting Information Table SI shows the average and standard deviation of $L_{n,0}$ for these three replicates. Although the order of magnitude of these equilibrium constants is highly reproducible, the coefficient has between 29 and 55% uncertainty, which is likely a better representation of the reproducibility of the parameters than the fitting uncertainty presented in Table III.

DISCUSSION

Our studies, for the first time, reveal the assembly pathway for formation of *E. coli* ClpB hexamers in the absence of nucleotide. Here we show that *E. coli* ClpB resides in a monomer-dimer-tetramer-hexamer equilibrium in the absence of nucleotide at three different salt concentrations. Further, we report that *E. coli* ClpB hexamers, like *T. thermophilus* ClpB and *S. cerevisiae* Hsp104,[9,19] exhibit a short half-life in solution (several minutes or less). Although we do not have precise measures of the dissociation rate constants, our analysis does indicate that it occurs with a rate constant $>0.01\ s^{-1}$.

ClpB/Hsp104 disrupts disordered protein aggregates in collaboration with the DnaK/Hsp70 system.[6,44,45] These enzymes play important roles in cell survival during stress, such as heat shock. To date, the mechanism of ClpB catalyzed protein disaggregation remains unclear.

At the heart of this protein disaggregation function are many protein–protein interactions. These include ClpB self-association, ClpB interactions with protein aggregates, and protein–protein interactions between ClpB hexamers and components of the DnaKJE system of enzymes that are yet to be fully resolved.[6,44,45] Consequently, determination of the ClpB assembly mechanism is an imperative first step to quantitatively understand how ClpB collaborates with DnaKJE to dissociate large protein aggregates.

Here we show that ClpB forms monomers, dimers, tetramers, and hexamers in solution in the absence of nucleotide. The concentrations of each of these oligomers can be described as a function of the total ClpB monomer concentration. This can be accomplished using the reported parameters in Table III and the model written in Scientist (Micromath Research, St. Louis MO) provided in the Supporting Information.

The ability to predict the concentration of hexamers in experiments performed at different total ClpB monomer concentrations at a variety of [NaCl] will aid in the design and interpretation of a number of other experiments. For example, as shown in Figure 6(a) for 300 m*M* NaCl, ClpB dimers and tetramers are

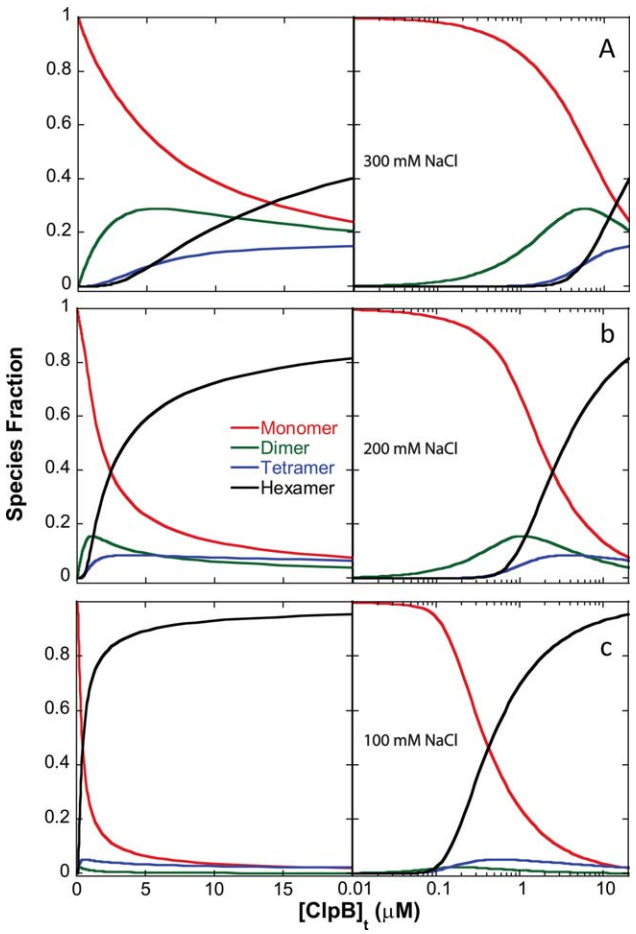

Figure 6

Species fractions simulations of ClpB. Simulations based on parameters determined in (**a**) 300 m*M* NaCl (**b**) 200 m*M* NaCl, and (**c**) 100 mM NaCl, monomer (red), dimer (green), tetramer (blue) and hexamer (black). Every panel is composed of two plots: The x axis is total ClpB monomer concentration, $[ClpB]_t$, and is presented in linear scale on the left and log scale on the right. The concentrations of ClpB oligomers are calculated using equilibrium constants presented in Tables III and IV. The simulations were generated using the Micromath Scientist model provided in the Supporting Information. ClpB oligomer concentration divided by the total ClpB concentration gives us the species fraction of that oligomer. The species fractions of these oligomers at various [NaCl] are presented.

significantly populated while hexamers are less populated. As the [NaCl] is decreased [Fig. 6(b,c)] ClpB hexamers become the most populated oligomer. This knowledge can be used to interpret kinetic data by accounting for the population of hexamers and other oligomers that may also contribute to the chaperone activity, such as ATP binding and hydrolysis or peptide binding and disaggregation.

As seen in Table III there is large uncertainty on the determination of the step-wise dimerization, K_2 and tetramerization, K_4, equilibrium constants in 100 m*M* NaCl when fitting to the 1–2–4–6 model. Yet the error on the hexamerization equilibrium constant, K_6, is much smaller. As shown in Figure 6(c), ClpB monomers and hexamers are significantly populated in 100 m*M* NaCl but dimers and tetramers are much more sparsely populated. Because monomers and hexamers are more highly populated the constraints on the hexamerization equilibrium constant, K_6, are much better than the dimerization, K_2, and tetramerization, K_4, equilibrium constants. However, because the stoichiometric assembly constants $L_{4,0}$ and $L_{6,0}$ are calculated using Eqs. (13) and (14), respectively, which are functions of the measured step-wise constants, the propagated uncertainties on those parameters are large. This observation would seem to imply that the sedimentation velocity data should be able to be described by a simple monomer-hexamer equilibrium. However, attempts to describe these data with the monomer-hexamer model resulted in and RMSD = 0.00989, which, based on F-statistics, is significantly worse than the 0.00965 reported in Table III for the 1–2–4–6 model.

One way to eliminate the dependence of the stoichiometric binding constants on the step-wise binding constants for ClpB assembly in 100 m*M* NaCl is using the stoichiometric model, "1–2, 1–4, 1–6," to analyze the data. However, the results presented here for 100 m*M* NaCl indicated that ClpB hexamer doesn't achieve instantaneous equilibrium on the time scale of sedimentation and the "1–2, 1–4, 1–6" model doesn't describe the data as well as the 1–2–4–6 model (see RMSD in Table III). Although the association rate constants for the "1–2, 1–4, 1–6" model make little sense, when the data are examined with this model with $L_{2,0}$, $L_{4,0}$, $L_{6,0}$ k_{r2}, k_{r4}, and k_{r6} floating, the fit describes the data equally well with an RMSD = 0.00964 as the 1–2–4–6 model. The dimerization constants floated to values consistent with an insignificant population and rapid dissociation, $L_{2,0} = 32.2\ M^{-1}$ and $k_{r2} = 258\ s^{-1}$, consistent with an insignificant population. Thus, the data are really being fit to a "1–4, 1–6" model and the determined parameters are $L_{4,0} = 3.4\ (2.8, 4.0) \times 10^{18}\ M^{-3}$, $L_{6,0} = 4.5\ (4.0, 5.0) \times 10^{32}\ M^{-5}$, $k_{r4} = 3\ (2, 6) \times 10^{-3}\ S^{-1}$, and $k_{r6} = 0.9\ (0.8, 1.1) \times 10^{-3}\ S^{-1}$. These results agree well with the parameters determined using a 1–2–4–6 model with an error space suggesting better constraints.

ClpB forms hexamer in the absence of nucleotide

There exist conflicting conclusions in the literature regarding whether ClpB forms hexamers or heptamers in the absence of nucleotide. It was reported by many groups that *E. coli* ClpB forms heptamers in the absence of nucleotide.[14,15,18] Akoev *et al.* concluded that ClpB resided in a monomer-dimer-heptamer equilibrium in the absence of nucleotide and the binding of nucleotide resulted in a conformational switch of ClpB from heptamer to hexamer.[14] However, del Castillo *et al.* reported that their experimental data for ClpB assembly can best be described by a monomer-hexamer-dodecamer model in the absence of nucleotide.[13]

Rigorously determining the assembly state for a polydisperse system is challenging. Previously published results on ClpB[17] and our experimental data (see Fig. 2) show that [NaCl] perturbs the ClpB assembly equilibrium. Therefore, we varied the [ClpB] and [NaCl] to find a condition that favors monodispersity. In buffer H supplemented with 100 m*M* NaCl, one predominant c(s) peak was found with an $s_{20,w} \sim 17.6$ S at multiple [ClpB] ranging from 4 to 18 μM.

Finding conditions where the system is monodisperse allowed us to determine the molecular weight of this 17.6 S species using sedimentation equilibrium experiments. We showed that the experimentally determined molecular weight of the ~17.6 S oligomer is ~578 kDa (see Figs. 3 and 4), which is in good agreement with the molecular weight of hexameric ClpB calculated from its primary structure. del Castillo *et al.* observed a population of oligomers with high sedimentation coefficients at high [ClpB] that they hypothesized may be a dodecamer. In our experimental [ClpB] range, no significant population of ClpB dodecamer is observed. However, the concentrations in our study are lower than those used by del Castillo. We avoided [ClpB] above 18 μM monomeric concentration to limit the impact on the data from effects of nonideality and nonspecific aggregation. Moreover, the physiological concentration of ClpB in *E. coli* reported by Mogk *et al.* is in the range of ~9–19 μM monomers.[46]

ClpB hexamer exhibits rapid dissociation

Here, in the absence of nucleotide, we report that ClpB oligomers exhibit rapid dissociation. In most cases, from this analysis, we do not have precise determinations of the rate constants. However, the analysis does reveal kinetic information and allows us to put a lower limit on the dissociation rate constants. For 300 and 200 m*M* NaCl all of the reactions occur with a dissociation rate constant of $\geq 0.01\ s^{-1}$. In the case of 100 m*M* NaCl the dissociation rate constant for hexamers was found to be within the measurable range and determined to be $\sim 1.3 \times 10^{-3}\ s^{-1}$.

The lower limits of the dissociation rate constants, which represent protein concentration-independent kinetic parameters, were determined from global fitting of sedimentation velocity experiments at multiple ClpB concentrations. Further, by combining the determined equilibrium constant with the lower limit of the dissociation rate constant, we can approximate the lower limits of the association rate constants for each bimolecular step, which represents the protein concentration-dependent kinetic parameter [see k_f in Eqs. (15)–(17)]. Therefore, a lower limit on the subunit exchange rate could be calculated as the product of the free ClpB concentration and the bimolecular rate constant, k_f.

The kinetics of subunit exchange for the hexamer of *T. thermophilus* ClpB[19] and *S. cerevisiae* Hsp104[9] has been examined by others using a stopped-flow FRET strategy. In those experiments, donor-labeled ClpB is rapidly mixed with acceptor-labeled ClpB. The donor- and acceptor-labeled ClpB must dissociate and then reassociate. Upon reassociation a FRET signal will be observed. The kinetic time courses acquired at a single protein concentration were examined by nonlinear-least squares fitting to a sum of three exponentials. The observed rate constants were reported as the rate constants for dissociation of the hexamer. However, it is clear from the work presented here that there are multiple oligomers present in solution that could contribute to this signal. Moreover, the reported apparent rate constant is a convolution of both dissociation and reassociation. Thus, to fully understand the mechanism of assembly, an examination of the dependence of this observed rate constant on protein concentration is still needed.

Several groups have employed gel filtration methods to examine ClpB assembly.[10,17,18,47] One study suggested that *E. coli* ClpB forms tetramers in the absence of nucleotide. This conclusion was drawn from the observation of a single elution peak with a retention time corresponding to a molecular weight of ~350 kDa, although the chromatogram was not shown.[47] These gel filtration experiments were performed under low salt conditions where our experiments would predict hexamer is the predominantly populated species. Thus, one explanation for the discrepancy between the gel filtration results and our findings would be that ClpB hexamer is rapidly dissociating and reassociating during the run. The free monomers, intermediate oligomers, and hexamers are separated by the gel-filtration column. The hexamers are further dissociated because the smaller oligomers and monomers are more and more separated as the sample moves through the column.

Because the kinetic properties of ClpB assembly were not largely discussed before the studies performed by Werbeck *et al.*[19] the dissociation kinetics of ClpB were not included in the interpretation of the gel filtration elution profiles for ClpB. In fact, the broadening of the elution peak can represent ClpB dissociation during the gel filtration run, which is similar to what we observe in c(s) distributions. That is to say, peaks in a c(s) distribution will be broadened if the macromolecule dissociates on the time scale of sedimentation at low ClpB concentrations. Indeed, the c(s) distributions can exhibit broadening for other reasons. Nevertheless, just as our analysis of the difference curves by incorporating kinetics, so too can the gel filtration elution profiles for ClpB be analyzed by incorporating kinetic parameters.[48–51] However, to our knowledge, this analysis has not been applied to the examination of ClpB using gel filtration.

The contribution of our work compared to a similar study performed by del Castillo *et al.*[13] is that we incorporated the kinetics of oligomerization into the data analysis and determined a pathway to describe ClpB hexamer assembly. Moreover, our reported association equilibrium constants for ClpB hexamers are several orders of magnitude greater than theirs. For example, they report a $K_6' = 10^{13}\ M^{-5}$ (in our notation and by our interpretation of their results this is $L_{6,0}$) at 150 m*M* KCl and as can be seen in Table III for 200 m*M* NaCl and 100 m*M* NaCl we determined an $L_{6,0} = \sim 10^{29}$ and $10^{33}\ M^{-5}$, respectively. Although the solution conditions employed by del Castillo *et al.* and us are not identical, with their reported numbers, the concentration of hexamers in solution would be predicted to be 7.8×10^{-23} μM for 10 μM total ClpB monomer concentration in the presence of 150 m*M* KCl. This concentration of hexamers is clearly under the detection limits of analytical ultracentrifugation experiments and in direct conflict with the raw data reported in their manuscript.[13]

The standard state Gibbs free energy change, $\Delta G^\circ_{6,}$ for ClpB hexamers formed through monomers can be calculated using Eq. (18):

$$\Delta G_6^\circ = -RT\ln(L_{6,0}) \tag{18}$$

where R is the gas constant and T is the absolute temperature. Using the $L_{6,0}$ presented in Table III, the ΔG°_6 is -190 kJ mol^{-1}, -167 kJ mol^{-1}, and -146 kJ mol^{-1} at 100, 200, and 300 m*M* NaCl, respectively. Our values are significantly smaller than those reported by del Castillo *et al.*[13] Nevertheless, our findings show that the formation of hexamers in the absence of nucleotide is energetically favored in solution.[10]

In this article, we presented a strategy to quantitatively investigate the energetics and kinetics of a large motor protein assembly, a strategy that can be employed to examine other AAA+ protein complexes. These proteins include a diverse array of molecular machines that are engaged in a variety of cellular activities.[2] As pointed out by many researchers, to fully understand the function of a protein machine, we not only need to know the structure at an atomic level, but also need to have knowledge of the energetics and kinetics for each intermediate step in the motor reaction.[52,53]

ACKNOWLEDGMENTS

We would like to thank Dr. Rebecca Wade and Axel Mogk for providing the ClpB hexamer structure model; thanks to Dr. Peter Prevelige for use of the XL-A analytical ultracentrifuge. Thanks to Dr. Walter Stafford for the XL-I analytical ultracentrifuge. Thanks to Hongyi Yang for discussions on structural analysis using VMD. Thanks to Elizabeth Duran, Nate Scull, and Ryan Stafford for comments on the manuscript. Special thanks to Francis Appling and Clarissa Weaver for critical reading of the manuscript. This work was supported by NSF grant MCB-1412624 to ALL.

REFERENCES

1. Arlt H, Tauer R, Feldmann H, Neupert W, Langer T. The YTA10-12 complex, an AAA protease with chaperone-like activity in the inner membrane of mitochondria. Cell 1996;85:875–885.
2. Neuwald AF, Aravind L, Spouge JL, Koonin EV. AAA+: a class of chaperone-like ATPases associated with the assembly, operation, and disassembly of protein complexes. Genome Res 1999;9:27–43.
3. Vale RD. AAA proteins. Lords of the ring. J Cell Biol 2000;150:F13–F19.
4. Motohashi K, Watanabe Y, Yohda M, Yoshida M. Heat-inactivated proteins are rescued by the DnaK.J-GrpE set and ClpB chaperones. Proc Natl Acad Sci USA 1999;96:7184–7189.
5. Genevaux P, Georgopoulos C, Kelley WL. The Hsp70 chaperone machines of *Escherichia coli*: a paradigm for the repartition of chaperone functions. Mol Microbiol 2007;66:840–857.
6. Glover JR, Lindquist S. Hsp104, Hsp70, and Hsp40: a novel chaperone system that rescues previously aggregated proteins. Cell 1998;94:73–82.
7. Schmitt M, Neupert W, Langer T. The molecular chaperone Hsp78 confers compartment-specific thermotolerance to mitochondria. J Cell Biol 1996;134:1375–1386.
8. Shorter J. Hsp104: a weapon to combat diverse neurodegenerative disorders. Neuro-Signals 2008;16:63–74.
9. DeSantis ME, Leung EH, Sweeny EA, Jackrel ME, Cushman-Nick M, Neuhaus-Follini A, Vashist S, Sochor MA, Knight MN, Shorter J. Operational plasticity enables hsp104 to disaggregate diverse amyloid and nonamyloid clients. Cell 2012;151:778–793.
10. Zolkiewski M, Kessel M, Ginsburg A, Maurizi MR. Nucleotide-dependent oligomerization of ClpB from *Escherichia coli*. Protein Sci 1999;8:1899–1903.
11. Veronese PK, Stafford RP, Lucius AL. The *Escherichia coli* ClpA molecular chaperone self-assembles into tetramers. Biochemistry 2009;48:9221–9233.
12. Li T, Lucius AL. Examination of polypeptide substrate specificity for *E. coli* ClpA. Biochemistry 2013;52:4941–4954.
13. del Castillo U, Alfonso C, Acebron SP, Martos A, Moro F, Rivas G, Muga A. A quantitative analysis of the effect of nucleotides and the M domain on the association equilibrium of ClpB. Biochemistry 2011;50:1991–2003.
14. Akoev V, Gogol EP, Barnett ME, Zolkiewski M. Nucleotide-induced switch in oligomerization of the AAA+ ATPase ClpB. Protein Sci 2004;13:567–574.
15. Kim KI, Cheong GW, Park SC, Ha JS, Woo KM, Choi SJ, Chung CH. Heptameric ring structure of the heat-shock protein ClpB, a protein-activated ATPase in *Escherichia coli*. J Mol Biol 2000;303:655–666.
16. Lee S, Sowa ME, Watanabe YH, Sigler PB, Chiu W, Yoshida M, Tsai FT. The structure of ClpB: a molecular chaperone that rescues proteins from an aggregated state. Cell 2003;115:229–240.
17. Schlee S, Groemping Y, Herde P, Seidel R, Reinstein J. The chaperone function of ClpB from *Thermus thermophilus* depends on allosteric interactions of its two ATP-binding sites. J Mol Biol 2001;306:889–899.
18. Mogk A, Schlieker C, Strub C, Rist W, Weibezahn J, Bukau B. Roles of individual domains and conserved motifs of the AAA+ chaperone ClpB in oligomerization, ATP hydrolysis, and chaperone activity. J Biol Chem 2003;278:17615–17624.
19. Werbeck ND, Schlee S, Reinstein J. Coupling and dynamics of subunits in the hexameric AAA+ chaperone ClpB. J Mol Biol 2008;378:178–190.
20. Schlieker C, Weibezahn J, Patzelt H, Tessarz P, Strub C, Zeth K, Erbse A, Schneider-Mergener J, Chin JW, Schultz PG, Bukau B, Mogk A. Substrate recognition by the AAA+ chaperone ClpB. Nat Struct Mol Biol 2004;11:607–615.
21. Lee S, Choi JM, Tsai FT. Visualizing the ATPase cycle in a protein disaggregating machine: structural basis for substrate binding by ClpB. Mol Cell 2007;25:261–271.
22. Haslberger T, Zdanowicz A, Brand I, Kirstein J, Turgay K, Mogk A, Bukau B. Protein disaggregation by the AAA+ chaperone ClpB involves partial threading of looped polypeptide segments. Nat Struct Mol Biol 2008;15:641–650.
23. Li T, Lin J, Lucius AL. Examination of polypeptide substrate specificity for *Escherichia coli* ClpB. Proteins 2015;83:117–134.
24. Li T, Weaver CL, Lin J, Duran EC, Miller JM, Lucius AL. *E. coli* ClpB is a non-processive polypeptide translocase. The Biochemical Journal 2015;470:39–52.
25. Laue TM, Shah BD, Ridgeway TM, Pelletier SL. Computer-aided interpretation of analytical sedimentation data for proteins. In: Harding SE, Rowe AJ, Horton JC, editors. Analytical ultracentrifugation in biochemistry and polymer science. Cambridge, England: Royal Society of Chemistry; 1992.
26. Laue TM, Shah BD, Ridgeway TM, Pelletier SL. Analytical ultracentrifugation in biochemistry and polymer science. Cambridge: Royal Society of Chemistry; 1992.
27. Lohman TM, Chao K, Green JM, Sage S, Runyon GT. Large-scale purification and characterization of the *Escherichia coli* rep gene product. J Biol Chem 1989;264:10139–10147.
28. Schuck P. Sedimentation analysis of noninteracting and self-associating solutes using numerical solutions to the Lamm equation. Biophys J 1998;75:1503–1512.
29. Schuck P, Rossmanith P. Determination of the sedimentation coefficient distribution by least-squares boundary modeling. Biopolymers 2000;54:328–341.
30. Ghirlando R, Balbo A, Piszczek G, Brown PH, Lewis MS, Brautigam CA, Schuck P, Zhao H. Improving the thermal, radial, and temporal accuracy of the analytical ultracentrifuge through external references. Anal Biochem 2013;440:81–95.
31. Zhao H, Ghirlando R, Piszczek G, Curth U, Brautigam CA, Schuck P. Recorded scan times can limit the accuracy of sedimentation coefficients in analytical ultracentrifugation. Anal Biochem 2013;437:104–108.
32. Schuck P. Size-distribution analysis of macromolecules by sedimentation velocity ultracentrifugation and Lamm equation modeling. Biophys J 2000;78:1606–1619.
33. Correia JJ. Analysis of weight average sedimentation velocity data. Methods Enzymol 2000;321:81–100.
34. Cole JL. Analysis of heterogeneous interactions. Methods Enzymol 2004;384:212–232.
35. Cole JL. Characterization of human cytomegalovirus protease dimerization by analytical centrifugation. Biochemistry 1996;35:15601–15610.
36. Veronese PK, Lucius AL. Effect of temperature on the self-assembly of the *Escherichia coli* ClpA molecular chaperone. Biochemistry 2010;49:9820–9829.
37. Ortega A, Amoros D, Garcia de la Torre J. Prediction of hydrodynamic and other solution properties of rigid proteins from atomic- and residue-level models. Biophys J 2011;101:892–898.

38. Oguchi Y, Kummer E, Seyffer F, Berynskyy M, Anstett B, Zahn R, Wade RC, Mogk A, Bukau B. A tightly regulated molecular toggle controls AAA+ disaggregase. Nat Struct Mol Biol 2012;19:1338–1346.
39. Humphrey W, Dalke A, Schulten K. VMD: visual molecular dynamics. J Mol Graph 1996;14:27–38.
40. Stafford WF, Sherwood PJ. Analysis of heterologous interacting systems by sedimentation velocity: curve fitting algorithms for estimation of sedimentation coefficients, equilibrium and kinetic constants. Biophys Chem 2004;108:231–243.
41. Johnson ML, Straume M. Comments on the analysis of sedimentation equilibrium experiments. In: Schuster TM, Laue TM, editors. Modern analytical ultracentrifugation. Boston: Birkhauser; 1994. pp 37–65.
42. Schuck P. Sedimentation patterns of rapidly reversible protein interactions. Biophys J 2010;98:2005–2013.
43. Diamant S, Rosenthal D, Azem A, Eliahu N, Ben-Zvi AP, Goloubinoff P. Dicarboxylic amino acids and glycine-betaine regulate chaperone-mediated protein-disaggregation under stress. Mol Microbiol 2003;49:401–410.
44. Goloubinoff P, Mogk A, Zvi AP, Tomoyasu T, Bukau B. Sequential mechanism of solubilization and refolding of stable protein aggregates by a bichaperone network. Proc Natl Acad Sci USA 1999;96: 13732–13737.
45. Zolkiewski M. ClpB cooperates with DnaK, DnaJ, and GrpE in suppressing protein aggregation. A novel multi-chaperone system from *Escherichia coli*. J Biol Chem 1999;274:28083–28086.
46. Mogk A, Tomoyasu T, Goloubinoff P, Rudiger S, Roder D, Langen H, Bukau B. Identification of thermolabile *Escherichia coli* proteins: prevention and reversion of aggregation by DnaK and ClpB. EMBO J 1999;18:6934–6949.
47. Woo KM, Kim KI, Goldberg AL, Ha DB, Chung CH. The heat-shock protein ClpB in *Escherichia coli* is a protein-activated ATPase. J Biol Chem 1992;267:20429–20434.
48. Ackers GK. Molecular sieve studies of interacting protein systems. I. Equations for transport of associating systems. J Biol Chem. 1967; 242:3026–3034.
49. Hummel JP, Dreyer WJ. Measurement of protein-binding phenomena by gel filtration. Biochim Biophys Acta 1962;63:530–532.
50. Wilton R, Myatt EA, Stevens FJ. Analysis of protein–protein interactions by simulation of small-zone gel filtration chromatography. Methods Mol Biol (Clifton, N.J) 2004;261:137–154.
51. Winzor DJ. The development of chromatography for the characterization of protein interactions: a personal perspective. Biochem Soc Trans 2003;31:1010–1014.
52. Alberts B. The cell as a collection of protein machines: preparing the next generation of molecular biologists. Cell 1998;92: 291–294.
53. Bukau B, Horwich AL. The Hsp70 and Hsp60 chaperone machines. Cell 1998;92:351–366.
54. Roark DE. Sedimentation equilibrium techniques: multiple speed analyses and an overspeed procedure. Biophys Chem 1976;5: 185–196.
55. Durchschlag H. Specific volumes of biological macromolecules and some other molecules of biological interest. In: Hinz H-JR, editor. Thermodynamic data for biochemistry and biotechnology. Berlin: Springer-Verlag; 1986. pp 45–128
56. Gabrielson JP, Arthur KK, Kendrick BS, Randolph TW, Stoner MR. Common excipients impair detection of protein aggregates during sedimentation velocity analytical ultracentrifugation. J Pharma Sci 2009;98:50–62.